conditions of the system with closely spaced natural frequencies. The network performance is excellent in predicting the damage conditions accurately and efficiently, and the discrepancy between the network identification results and the desired output is within 1.7%.

3) In structural damage identification, this method allows one to have the option of selecting one or a few measurements in modal testing for the change of pole/zero as the input data of a diagnosis network. Compared with earlier work carried out by measuring the structural mode shapes, this method significantly simplifies the experimental loads in identifying the extent and location of complex damage conditions. Note that a comprehensive, complete, and relevant set of training data obtained either from numerical simulation or from modal testing for different damage scenarios is the basis of the neural-based scheme. The accuracy of the diagnosis network is usually proportional to the training cost. Further work may be necessary to reduce the required training data without degrading the network performance.

References

[1]Kudva, J. N., Munir, N., and Tan, P. W., "Damage Detection in Smart Structures Using Neural Networks and Finite-Element Analyses," *Smart Materials and Structures*, Vol. 1, 1992, pp. 108–112.

[2]Worden, K., Ball, A. D., and Tomlinson, G. R., "Fault Location in a Framework Structure Using Neural Networks," *Smart Materials and Structures*, Vol. 2, 1993, pp. 189–200.

[3]Szewczyk, Z. D., and Hajela, P., "Damage Detection in Structures Based on Feature-Sensitive Neural Networks," *Journal of Computing in Civil Engineering*, Vol. 8, pp. 163–178.

[4]Barai, S. V., and Pandey, P. C., "Performance of the Generalized Delta Rule in Structural Damage Detection," *Engineering Applications of Artificial Intelligence*, Vol. 8, 1995, pp. 211–221.

[5]Pandey, P. C., and Barai, S. V., "Multilayer Perceptron in Damage Detection of Bridge Structures," *Computers and Structures*, Vol. 54, 1995, pp. 597–608.

[6]Elkordy, M. F., Chang, K. C., and Lee, G. C., "A Structural Damage Neural Network Monitoring System," *Microcomputers in Civil Engineering*, Vol. 9, 1994, pp. 83–96.

[7]Ceravolo, R., Stefano, A. D., and Sabia, D., "Hierarchical Use of Neural Techniques in Structural Damage Recognition," *Smart Materials and Structures*, Vol. 4, 1995, pp. 270–280.

[8]Chen, S. S., and Kim, S., "Automated Signal Monitoring Using Neural Networks in a Smart Structural System," *Journal of Intelligent Materials Systems and Structures*, Vol. 6, 1995, pp. 508–515.

[9]Molas, G. L., and Yamazaki, F., "Neural Networks for Quick Earthquake Damage Estimation," *Earthquake Engineering and Structural Dynamics*, Vol. 24, 1995, pp. 505–516.

[10]Rhim, J., and Lee, S. W., "A Neural Network Approach for Damage Detection and Identification of Structures," *Computational Mechanics*, Vol. 16, 1995, pp. 437–443.

[11]Tsou, P., and Shen, M.-H. H., "Structural Damage Detection and Identification Using Neural Networks," *AIAA Journal*, Vol. 32, No. 1, 1994, pp. 176–183.

[12]Kirkegaard, P. H., and Rytter, A., "The Use of Neural Networks for Damage Detection and Isolation in a Steel Member," *Proceedings of Neural Networks and Combinatorial Optim. in Civil and Structural Engineering*, Civil-Comp Press, Edinburgh, Scotland, U.K., 1993, pp. 1–9.

[13]Islam, A. S., and Craig, K. C., "Damage Detection in Composite Structures Using Piezoelectric Materials," *Smart Materials and Structures*, Vol. 3, 1994, pp. 318–328.

[14]Kaminski, P. C., "The Approximate Location of Damage Through the Analysis of Natural Frequencies with Artificial Neural Networks," *Journal of Process Mechanical Engineering*, Vol. 209, 1995, pp. 117–123.

[15]Ferregut, C. M., Osegueda, R. A., and Ortiz, J., "Artificial Neural Networks for Structural Damage Detection and Classification," *Proceedings of SPIE–The International Society for Optical Engineering*, Vol. 2446, 1995, pp. 68–80.

[16]Yang, S. M., and Lee, G. S., "Vibration Control of Smart Structures by Using Neural Networks," *Journal of Dynamic Systems, Measurement and Control*, Vol. 119, No. 1, 1997, pp. 34–39.

[17]Kabe, A. M., "Stiffness Matrix Adjustment Using Mode Data," *AIAA Journal*, Vol. 23, 1985, pp. 1431–1436.

G. A. Kardomateas
Associate Editor

Noncontact Electron Gun Strain Control of Piezoceramics

George C. Nelson* and John A. Main†
University of Kentucky, Lexington, Kentucky 40506-0108

Introduction

STRAIN control in piezoceramics requires the application of external electric fields to the active material. This has traditionally been accomplished by sandwiching the material between conducting electrodes. The electrodes are appropriately segmented to control individual areas of the actuator (Fig. 1). Although effective, there are definite constraints on using electrodes to accomplish strain control in piezoelectric materials. Application of electric fields to piezoelectric materials in this way may become impractical as the controlled area increases and the spatial resolution becomes finer. In such cases the number of electrodes and leads will become very large.

One possible solution to this problem is to deposit control charges directly onto the surface of the piezoelectric material with an electron gun. An obvious advantage of this method, if it proves to be practical, is that only the electron beam size and the properties of the driven structure will limit spatial resolution.

The idea of applying control charges with an electron gun to stimulate piezoelectric response was put forth in an invention description by Brown and Sivyer.[1] They outlined the design of an acoustic transducer that uses an electron gun to excite a piezoelectric layer. This work stressed dynamic excitation of the piezoelectric material structure rather than strain control. More recently Hubbard[2] described an electron gun system to actuate a wavefront correction mirror constructed from a glass/polyvinylidene fluoride (PVDF) laminate. This is the work most directly relevant to the current investigation because strain control of the piezoelectric structure was emphasized. Hubbard's control method is described and compared to the method used in this investigation in the following technical description.

The most attractive feature of electron gun control is the absence of the constraining electrode pattern in the structure. In theory the electron gun can apply a charge distribution of any size and shape to any location on a distributed structure. This is a significant advantage when extremely large active or smart structures are under consideration for precision applications. The ability to build an active structure without electrode patterns and lead wires greatly increases the options open to the system designer.

If a practical method of shape control of large surfaces with fine spatial resolution is developed a number of applications suggest themselves. Possibilities abound in the areas of acoustics and instrumentation. A particularly intriguing application is large optical mirror structures for space applications. If an extremely precise active structural system capable of maintaining a desired shape to optical tolerances could be constructed, then space telescope mirrors of enormous size might be possible. The flexible nature of electron gun control may make it possible to construct these structures in segments and assemble them on orbit, or perhaps stow them as a furled thin film and deploy them and then tune the structure to a precise optical shape. This is, of course, an extremely bold proposal, and proving such a concept feasible is a task well beyond the scope of the work described herein. This Note is intended only to begin the understanding of the important physics associated with electron gun control of piezoelectric strains.

Received 16 August 1999; revision received 16 October 2000; accepted for publication 6 April 2001.

*Research Assistant, Department of Mechanical Engineering, 521 CRMS Building. Member AIAA.

†Associate Professor, Department of Mechanical Engineering, 521 CRMS Building. Member AIAA.

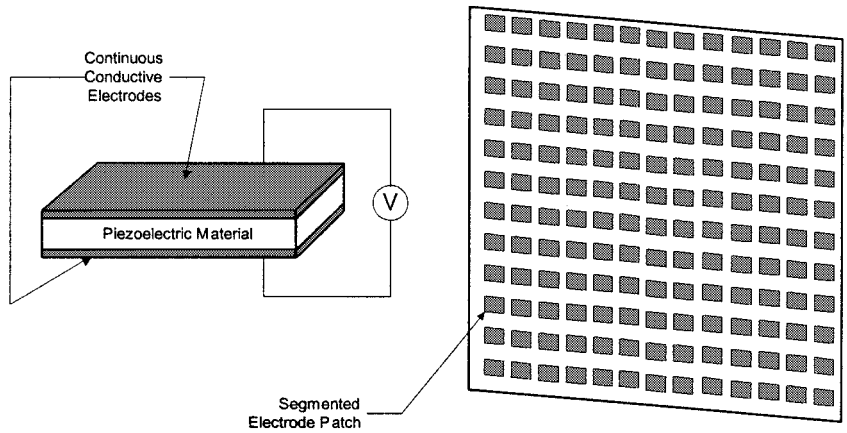

Fig. 1 Control of a distributed piezoelectric structure with segmented electrodes requires a separate electrode and lead for each discrete area to be controlled.

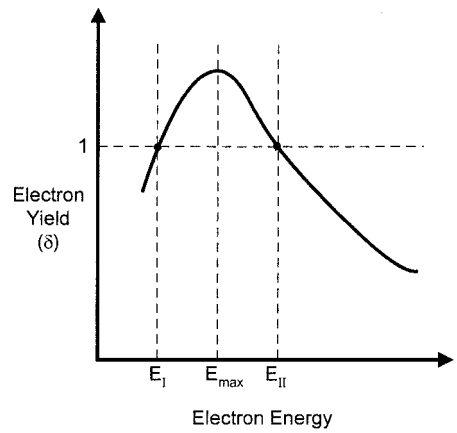

Fig. 2 Typical secondary electron emission curve for a dielectric material.[3]

Physics of Secondary Electron Emission

Placing charge from an electron gun on the surface of a dielectric to stimulate piezoelectric response is not as simple as aiming the gun and shooting the charge where desired. The surface charge changes in response to the collision of an electron with the surface, but the change is not the addition of one electron. An electron is decelerated when it impacts a surface, giving up kinetic energy to the material. A number of things can happen to that energy, including raising the energy levels of other electrons to the point that they are ejected from the surface.

Figure 2 shows the secondary electron yield for a typical dielectric material as a function of the incident electron energy.[3] The yield curve for most materials is generally of this shape. The consistency in shape across materials is such that the curves themselves are typically characterized by three parameters: the two crossover points where the electron yield δ equals unity and the energy where the electron yield is at a maximum. The two crossover energies are conventionally labeled E_I and E_{II}. This is somewhat simplistic, however, because the yield of some materials never reaches one, in which case E_I and E_{II} are undefined, whereas other materials may have a defined E_I and no E_{II}.

Assume that a material is experiencing an electron flux and it has a secondary emission curve with a defined E_I and E_{II}. When the impact energy of the primary electrons, E_p, falls in a region with an electron yield greater than one ($E_I < E_p < E_{II}$), there is a net flow of electrons off the surface, and positive charge accumulates if there is a collector present that is positive with respect to the surface. If $E_p < E_I$ the surface charges negatively in the direction of the potential of the electron source. If $E_p > E_{II}$, then the surface charges to the potential that would decelerate an electron to E_{II}. The voltage known as the sticking potential represents the maximum voltage the surface can reach due to the electron flux.[4]

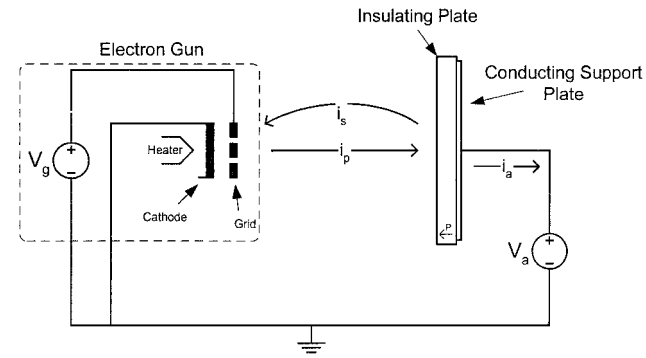

Fig. 3 Schematic of the electron gun plate applying an electron flux to an insulating plate.

A schematic representing an insulating, piezoelectric plate being subjected to current from an electron gun is shown in Fig. 3. The labeled currents represent the primary electron current i_p, the secondary electron current back to the grid i_s, and the net circuit current i_a. The three currents are related by

$$i_a = i_p - i_s \tag{1}$$

Note that these are electron currents rather than conventional current. The two labeled potentials are the accelerating voltage applied to the electrons, V_g, and the potential of a conducting support plate mounted on the back of the piezoelectric plate, V_a. The accelerating potential and resulting electron energy are related as follows: a V_g of 500 V will generate an electron stream with energy 500 eV at the outlet of the electron gun.

The ultimate goal is to control the strain in the piezoelectric material. This means the electric field across the plate must be controlled. The potential of one side of the plate is directly controlled by the voltage source V_a. The remaining challenge is to control the potential of the surface facing the electron gun, V_s, and thereby control the electric field in the material.

Bruining[5] presents a method for analyzing the Fig. 3 circuit that includes the secondary emission characteristic. Figure 4 is adapted from Ref. 5. The curve labeled I in Fig. 4 is the relationship between the net circuit current i_a and the energy of the electron at impact given in terms of an accelerating potential V_p. This curve is related to the secondary electron yield curve for a given material and is referred to as the dynatron characteristic. Bruining treats the insulating plate as a conductor of very high resistance for the purposes of this analysis. Line II is the resistance line showing the electrical behavior of the insulating plate when the potential of the supporting conductive plate is V_a.

The potential of the surface of the plate facing the electron gun must be determined to relate this analysis to piezoelectric strain. This can be accomplished by first noting that the energy of the electron as it exits the gun assembly is given by

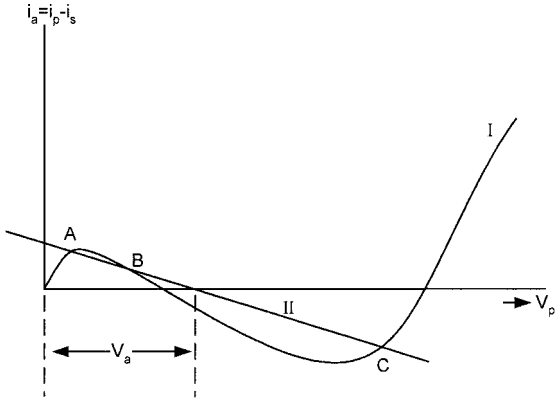

Fig. 4 Possible solutions A, B, and C for a typical dynatron characteristic (I) and the dielectric plate resistance line (II).[5]

$$E_g = V_g(q) \tag{2}$$

where V_g is the accelerating voltage of the electron gun and q is the charge of an electron. The energy the primary electron possesses when it impacts the piezoelectric plate is

$$E_p = V_p(q) \tag{3}$$

where V_p is the potential required to accelerate an electron to kinetic energy E_p.

Between exiting the electron gun and impacting the piezoelectric plate, the electron experiences a change in kinetic energy due to the potential difference between the accelerating grid and the surface of the insulating plate. This is ΔE and is defined as

$$\Delta E = (V_s - V_g)(q) \tag{4}$$

where V_s is the potential of the surface of the insulating plate.

The total energy the primary electrons possess when they strike the surface of the insulating, piezoelectric plate is, therefore,

$$E_p = E_g + \Delta E = V_s(q) \tag{5}$$

Combining Eqs. (3) and (5) shows that the surface potential of the insulating plate V_s is also the accelerating potential in Fig. 4, V_p:

$$V_s = V_p \tag{6}$$

and the strain in the unconstrained piezoelectric plate ε is

$$\varepsilon_k = d_{jk}(V_a - V_s)/t \tag{7}$$

where t is the plate thickness, d is the piezoelectric constant, and the subscript j corresponds to the thickness direction.

In Fig. 4 the intersections of curves I and II, labeled A, B, and C, represent possible system equilibrium points, and only A and C are the possible stable equilibria. Point B is unstable because any decrease in V_p causes the surface potential to decrease. This effectively lowers V_p further and on and on until the system reaches point A. A similar analysis shows that positive V_p deviations from point B lead the system to stable equilibrium C.

The secondary emission curve must be known for the material to determine precise equilibrium conditions. These curves are available for most elements, and occasionally the literature includes secondary emission data for other materials. For example, the secondary emission curve for the piezoelectric polymer PVDF was determined by Koshida and Yoshida.[6] The secondary emission curve for PZT-5H, the material used in the experiments described in this paper, was not evident in a search of the literature. PZT was used in this investigation rather than the thin-film PVDF because strain gauges could be bonded to the material to measure induced strains directly. The critical points on the secondary yield curve are noted in Table 1 for the three principal components of PZT, lead (Pb), zirconium (Zr), and titanium (Ti) (Ref. 3). However, the secondary electron yields of compounds are generally different than those of their constituent elements.[5] Bruining points out that the determination of the system equilibrium is difficult even if the secondary yield curves are known because of the assumptions that the secondary yield behavior is invariant with respect to the electric field in the material and that the plate resistance is well defined. Bruining also states that in reality the plate resistance is not constant but is a function of i_a.

Table 1 Secondary emission properties of lead, zirconium, and titanium[3]

Element	Maximum secondary yield (δ_{max})	Energy at maximum yield	E_I	E_{II}
Pb	1.1	500	250	1000
Zr	1.1	350	175 (Ref. 5, p. 38)	
Ti	0.9	280	None	None

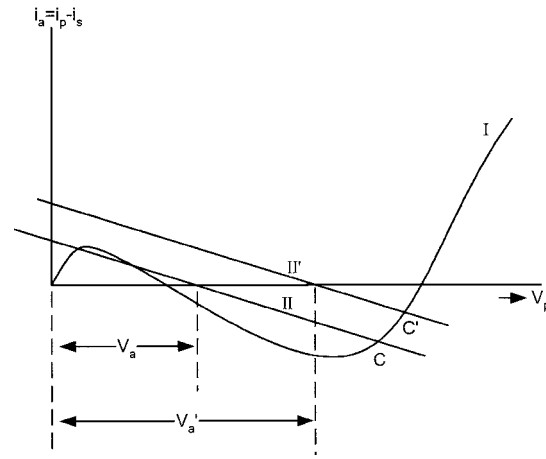

Fig. 5 Effect of increase in the potential of the electrode V_a on the surface potential.[5]

Although quantitative predictions are difficult to make, Bruining's[5] analysis is still useful for analyzing and formulating methods to control the electric field in the piezoelectric plate shown in Fig. 3. Hubbard[2] developed a system for strain control of a piezoelectric plate using a hardware setup similar to Fig. 3. The control approach was to use electron beams of different energies to apply (+) or (−) charges to stimulate strains. To achieve this, V_g was varied while V_a remained constant. When Fig. 4 is referred to, application of positive charge to the surface requires an electron beam with an initial V_g between the middle zero point in curve I and point C. This increases the potential of the surface of the piezoelectric plate, which further accelerates the electrons and increases their energy. The system reaches equilibrium at point C. When Bruining's[5] resistive element analysis is used, this means that the potential of the surface is positive relative to V_a.

Generating a negative potential on the surface requires an electron beam with energy such that electrons are delivered to the surface with energy falling between intersection A and the middle zero point of curve I. Point A is the stable equilibrium point when the electron beam is in this energy range. The result of applying electrons in this energy range is that the surface potential becomes negative relative to V_a.

Hubbard[2] described obtaining intermediate values of surface potential, and thus piezoelectric strain, between the two equilibrium states described earlier by applying electrons from one of two energy levels and stopping the electron current before the equilibrium state was reached. Low-energy electrons were used to drive the system toward equilibrium A, and high-energy electrons were used to drive the system toward equilibrium C. One unfortunate characteristic of this control approach is that the system state is not necessarily at a stable equilibrium point. Hubbard noted that this approach exhibited instabilities, and signal processing was required for predictable operation.

Bruining[5] provides a clue to solving the instability problems encountered by Hubbard.[2] Improved system stability is generally desirable, though it is often gained at the cost of slower system response. Figure 5 shows an excerpt from the analysis of the Fig. 3 circuit illustrating the relationship between the system equilibrium points and the potential of the conductive plate, V_a. Assume that

an electron stream is applied to the piezoelectric material surface and the energy of the electrons is such that the system stabilizes at point C. If the conductive plate potential V_a is then increased, the new resistance line is II′ and the equilibrium point moves to C′. This results in a new surface potential V_s at this equilibrium point. As long as V_a and V_s do not experience identical changes, the electric field in the piezoelectric plate can be changed continuously by varying V_a, and the system will always be at a stable equilibrium.

Experimental Protocol and Results

The noncontact, electron gun control scheme for strain control of piezoelectric structures outlined in the preceding section was experimentally evaluated to explore system response to a variety of inputs. The material used throughout the investigation was a 7.6 cm $\times$ 5 cm $\times$ 1.9 mm (3 $\times$ 2 $\times$ 0.075 in.) thick plate of PZT-5H. The specimen had a silver electrode on both faces, and the material was poled in the thickness direction. Electrode thickness ranged from 0.0003 to 0.001 in. (7 to 25 μm). The positive electrode was removed with a combination of chemical etching and polishing to expose the bare face of the dielectric material.

A photograph of the interior of the vacuum chamber is shown in Fig. 6. A resistance strain gauge was bonded on top of the remaining electrode and oriented to detect strain in the 1 direction as shown in Fig. 7. A wire lead was soldered to the electrode and connected to a power amplifier capable of applying a V_a of $\pm$200 V. The piezoelectric plate was securely held at one end and placed in the vacuum chamber so that the unelectroded side was facing and perpendicular to the electron gun, which is a Kimball Physics EFG-7. The distance from the gun to the target was 12 cm (4.7 in.). The electron gun controller permits variation of beam energy, current, and focus. The beam diameter at the sample was kept constant at approximately 2.5 cm (1 in.), and x and y beam steering was accomplished with deflection plates. A phosphor screen was placed behind the PZT plate to provide visual feedback of an operating electron beam. Typical vacuum chamber pressures during experimentation ranged from 2.0e–6 to 5.0e–7 torr.

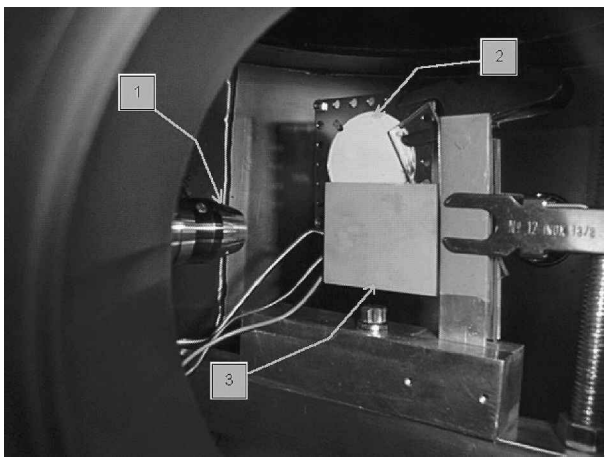

Fig. 6 Electron gun (1), phosphor screen for checking beam directional control (2), and the piezoelectric material target (3).

Because the secondary electron emission curve for PZT-5H was not available to determine the proper energy for stimulating secondary emissions, the elemental secondary emission characteristics in Table 1 were used as a general guide. For successful operation of the V_a control scheme, it is necessary to bombard the piezoelectric plate with electrons of energy greater than E_I and somewhat less than E_{II}. Of the three elements listed in Table 1 the highest E_I listed is for lead at 250 eV. The only E_{II} point defined is 1000 eV, also for lead. The electron energies used in the tests to be described were selected because they were at or above 250 eV and well below 1000 eV.

The material was assumed to be at zero stress and strain when first placed inside the vacuum chamber. The electron gun was first activated with the energy set at 250 eV and very low gun emission current (approximately 5 μA) with V_a set at ground potential. The precise current can be measured with a Faraday cup attachment on the electron gun, but this was not part of the experimental setup. On first exposure to the electron beam, the material responded with strains in the 1 direction on the order of 45 $\mu\varepsilon$ that remained in the material after the electron beam was shut off. A uniform initialization of the material at this strain level was accomplished by subjecting the entire actuator surface to the primary electron stream by manually varying the beam direction with the deflection plates. The strain instrumentation was rezeroed after the initialization. This initialization bias disappears if the material is exposed to atmospheric conditions because of discharge to the atmosphere.

After the initialization was completed, the 2.5-cm-diam beam was pointed to a location on the sample centered on the strain gauge location shown in Fig. 7. V_a was then varied between $-$200 and $+$200 V, and the strain in the 1 direction of the piezoelectric plate was recorded. The V_a input and strain response are shown as a function of time in Fig. 8a, and strain as a function of V_a is shown in Fig. 8b. The ratio of the magnitude of noise to the magnitude of measured strain in the plots presented here is approximately 7%.

The strain response to the V_a input shows evidence of the unstable strain-field behavior predicted for point B in Fig. 4. The plot starts at zero V_a and zero strain and increases linearly up to a maximum of 12 $\mu\varepsilon$. V_a is then decreased from the 200 V maximum, and the

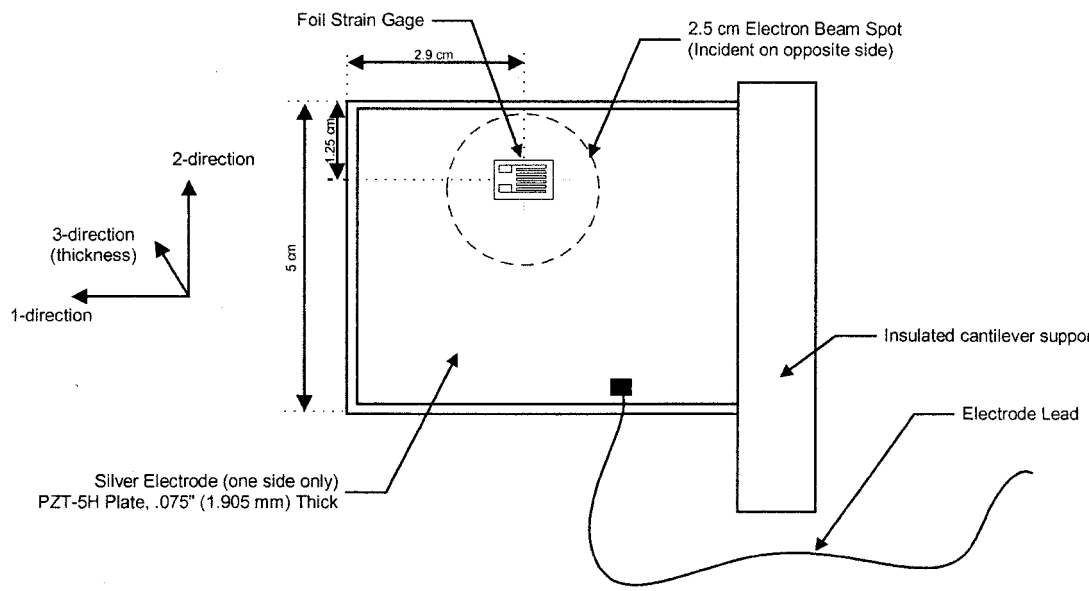

Fig. 7 Electron beam target and strain gauge location on the sample.

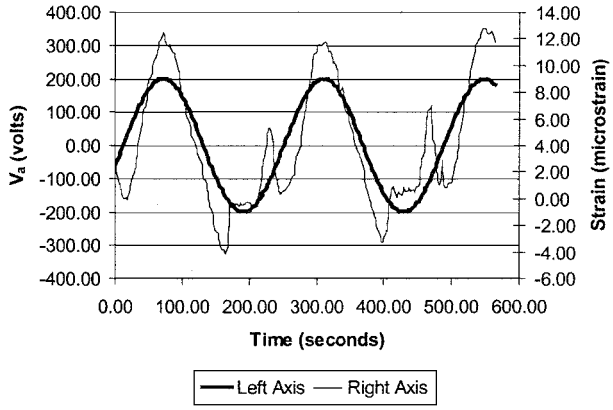

a) Function of time

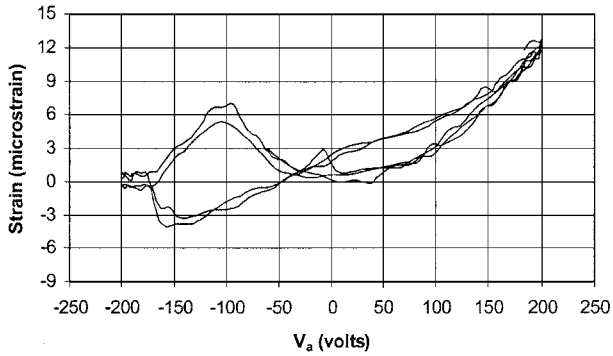

b) Strain vs V_a hysteresis loop for the 250-eV electron beam tests

Fig. 8 V_a input and piezoelectric response.

response remains linear until V_a reaches approximately −150 V. At this point the strain response abruptly changes directions and moves positive. This is indicative of net electron current swinging from negative to positive. In terms of the analysis in Fig. 4, this means that the resistance line is moved left to the point that there is no intersection at point C, and the only equilibrium point remaining is at point A. All response ceases at a V_a of −175 V because the negative surface potential is strong enough to choke off the incoming beam. No strain changes are seen in response to V_a inputs until it moves back above −175 V. The strain then increases in proportion to V_a until the response again abruptly swings negative and returns to the original starting point. This is indicative of the resistance line moving back to the right until the only remaining equilibrium point is point C.

The 250-eV electron beam test showed a linear response as long as V_a was greater than approximately −20 V. Because positive voltages accelerate electrons, the same linear response should be obtainable over a wider range by using a higher energy electron beam. The experiment was repeated with the beam energy increased to 300 eV. V_a was again cyclically varied from −200 to +200 V and the resultant strain recorded. The results from this test are shown in Figs. 9a and 9b. The response to the 300-eV beam is significantly more linear than the 250-eV response, but nonlinear behavior is still evident at the lowest applied voltages.

The test was then repeated with a beam of 400-eV electrons. The results of these tests are presented in Figs. 10a and 10b. The 400-eV results demonstrated a nearly proportional relationship between V_a and piezoelectric strain.

The persistence of the induced strains was then evaluated with the following test. At the beginning of the demonstration the gun is off, the V_a potential electrode is set to ground, and the strain is zeroed. Figure 11 shows V_a, beam state (on or off), and in-plane piezoelectric response as a function of time. At 10 s, the gun is activated, and a 200-V step is applied to the electrode, which resulted in approximately 11 $\mu\varepsilon$. At 100 s, the gun is turned off, opening the electric circuit, and V_a is returned to zero. Note that the strain remains in the material, and no signs of charge leakage are evident over the next

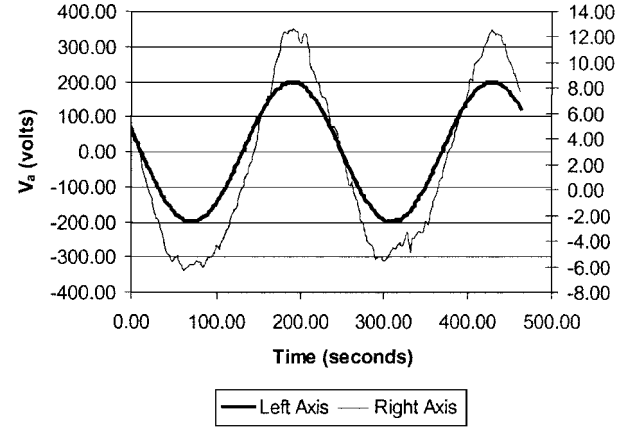

a) Function of time

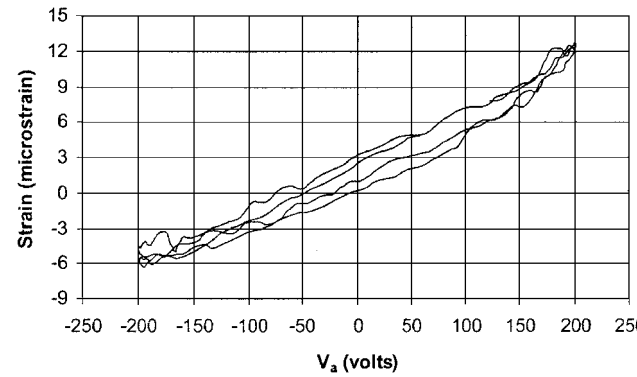

b) Strain vs V_a hysteresis loop for the 300-eV electron beam tests

Fig. 9 V_a input and piezoelectric response.

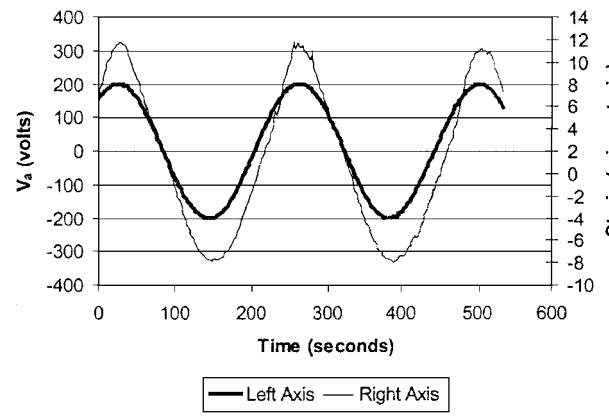

a) Function of time

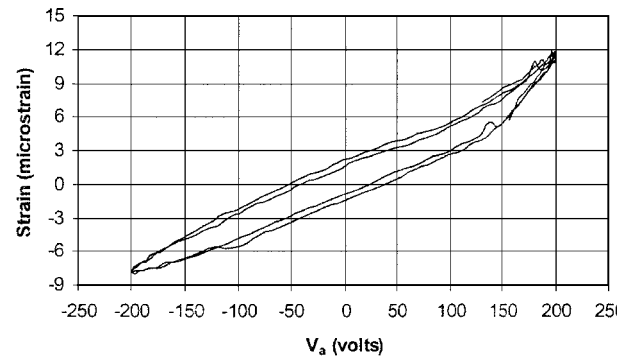

b) Strain vs V_a hysteresis loop for the 400-eV electron beam tests

Fig. 10 V_a input and piezoelectric strain response.

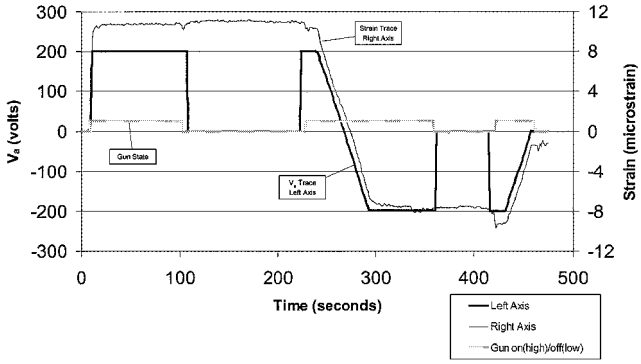

Fig. 11 Electron gun state V_a and resultant strain as a function of time. Note that the piezoelectric strain remains in the material for significant periods of time even with the gun deactivated and V_a is removed.

100 s. At 215 s, V_a is stepped back to the 200-V level, and the gun is turned on immediately thereafter. With the circuit reestablished, V_a is then ramped slowly to −200 V to generate a strain of −8 $\mu\varepsilon$. V_a and the gun current are then deactivated again to demonstrate the permanence of the shape changes. The current is then reestablished by returning to the original V_a, and gun current levels and the piezoelectric strain is ramped back toward zero. Clearly evident in this simple test are the controllability, reversibility, and short-term stability of piezoelectric strains stimulated by electron gun charge and V_a inputs.

Conclusions

Strain control of a piezoelectric plate using an electron gun to deposit charge on the bare face of the material and a single distributed electrode on the opposite side was demonstrated to be stable, controllable, and repeatable. The responses observed while using the 300- and 400-eV electron beams are similar in linearity and hysteresis to piezoelectric responses using the conventional paired electrode method. It was also demonstrated in tests using a 400-eV beam that charge input can be applied to the material and that the resultant strains will remain for a significant period of time after the removal of the electron beam. Clearly nonlinear behavior due to unstable points in the secondary emission curve were evident in the 250-eV beam tests, indicating that higher beam energies are more desirable for stable operation.

The electron beam shape control method appears to hold potential for applications requiring high-resolution shape control of a large structure with extremely high resolution. Given that electron guns require vacuum to operate effectively, space is obviously one place to look for potential applications. Two specific possible uses involve the gathering of light. First, solar thermal propulsion units could utilize the shape correction possibilities of an electron gun controlled mirror to gather and focus the desired solar radiation. Second, orbital telescopes used in cosmology or Earth observations could take advantage of the ability to control very large surface areas to optical tolerances. The advantage of a large telescope is that the more light that is gathered then the better the telescope performs. The manufacture of extremely large primary and secondary reflectors may become much easier and cheaper if a practical method of on-orbit shape correction can be developed and implemented. Based on the research performed to date, electron gun shape control of piezoelectric materials may provide one possible avenue for performing on-orbit shape tuning of extremely large optical components.

Acknowledgments

The authors gratefully acknowledge the support of the NASA Advanced Concepts Research Program (Cooperative Agreement NAG8-1317, Technical Monitors W. Brantley and W. Emrich), and the National Science Foundation (Grant CMS97-13952, Program Directors D. Garg and A. Flatau) for their support of this research. The authors also wish to thank Jeffrey Martin for his significant contributions to the development of the experimental apparatus used in this investigation. The candid, constructive comments made by the reviewers were also very valuable to the authors during the preparation of this Note.

References

[1] Brown, P. H., Sivyer, R. F., "Cathode Ray Tube Acoustic Transducers," U. S. Patent. 3,899,709, filed June 1974.

[2] Hubbard, J., "Active Mirror Assembly," U. S. Patent. 5,159,498, filed 22 Oct. 1992.

[3] *CRC Handbook of Chemistry and Physics*, 62nd ed., 1982, pp. E373, E374.

[4] Geppert, D., *Basic Electron Tubes*, McGraw–Hill, New York, 1954, pp. 202, 203.

[5] Bruining, H., *Secondary Electron Emission*, McGraw–Hill, New York, 1954, pp. 19–22, 29–57.

[6] Koshida, N., and Yoshida, S., "Secondary Electron Emission from Polyvinylidene Fluoride (PVDF) Film," *Japanese Journal of Applied Physics*, Vol. 22, No. 11, 1983.

A. M. Baz
Associate Editor

Improved Calculation of Eigenvalue Variation in Dynamic System

X. L. Liu*
Laboratório Nacional de Engenharia Civil, 1700-066 Lisbon, Portugal

Introduction

THE prediction of the modal change following a modification in a dynamic system is useful in many problems of engineering practice. This type of study was addressed as early as in Rayleigh's book.[1] It is noted that the formulas of either perturbation,[2,3] sensitivity,[4] or variation[5] are essentially of a similar form and hence they are considered as instances of the classic method. Normally, to improve the accuracy of an analysis, two ways are followed: the addition of higher variations and the utilization of an iterative process.[6,7] The step-by-step procedure based on the division of a large modification into small ones is an alternative.[7] The use of the Rayleigh quotient is a good way of approximation because it involves a second-order error.[2] Bickford[8] proposed a modified first variation, which can make up the Rayleigh quotient. The incorporation of the Rayleigh quotient into a perturbation analysis can also improve the convergence of the eigenvalues as well as the eigenvectors.[9,10]

A procedure for the improved calculation of eigenvalue variations is presented in this Note.

Classic Method

For a dynamic system in the original state, the eigenvalue equation is in a form of

$$\left(\boldsymbol{A}_0 - \lambda_{0_i}\boldsymbol{B}_0\right)\boldsymbol{x}_{0_i} = \boldsymbol{0} \tag{1}$$

where $\boldsymbol{A}_0$ and $\boldsymbol{B}_0$ are real symmetrical matrices and λ_{0_i} and $\boldsymbol{x}_{0_i}$ are ith eigenvalue and eigenvector, respectively. The orthonormality relationships can be defined as

$$\boldsymbol{x}_{0_i}^T\boldsymbol{A}_0\boldsymbol{x}_{0_j} = \delta_{ij}\lambda_{0_i} \tag{2}$$

$$\boldsymbol{x}_{0_i}^T\boldsymbol{B}_0\boldsymbol{x}_{0_j} = \delta_{ij} \tag{3}$$

Received 30 August 2000; revision received 28 November 2000; accepted for publication 24 January 2001.

*Assistant Researcher, Av. do Brasil, 101; liu@lnec.pt.